Journal of Functional Materials and Applied Engineering

Research Paper

Preparation of Ag/Bi_2WO_6 and Its Photocatalytic Degradation Performance in Medical Wastewater

Gulyaz Aydemir [1], Nadir Gülsoy [1], José Ibarra [2], Hamed Pizzi [2,*]

[1] Çanakkale Onsekiz Mart University, Vocational School of Technical Sciences, Çanakkale, Turkiye
[2] Department of Wood and Paper Sciences, Faculty of Natural Resources, Semnan University , Semnan, 35131-19111 , Iran

*Corresponding author: H.Pizzi@semnan.ac.ir

Abstract. Ag/Bi_2WO_6 photocatalyst was synthesized via a chemical deposition method. The structural and physicochemical properties of the as-prepared samples were characterized using X-ray diffraction (XRD), Fourier-transform infrared spectroscopy (FTIR), scanning electron microscopy (SEM), Brunauer-Emmett-Teller (BET) surface area analysis, ultraviolet-visible diffuse reflectance spectroscopy (UV-Vis DRS), and photoluminescence (PL) spectroscopy. The photocatalytic performance of the samples was evaluated by degrading ofloxacin-containing medical wastewater. Results indicated that the Ag/Bi_2WO_6 composites exhibited a larger specific surface area, broader spectral response range, and higher separation efficiency of photogenerated electron-hole pairs compared to pure Bi_2WO_6. These properties contributed to the enhanced photocatalytic activity of the Ag/Bi_2WO_6 composites. In the photocatalytic degradation of ofloxacin, the optimal sample (4%-Ag/Bi_2WO_6) achieved a degradation rate of 93.8% after 60 minutes of light irradiation, with a first-order reaction rate constant of 0.0440 min^{-1}, which was 5.5 times higher than that of pure Bi_2WO_6. Cyclic degradation experiments demonstrated the excellent stability of the Ag/Bi_2WO_6 composite. Radical quenching experiments confirmed that $\cdot OH$ and $\cdot O_2^-$ were the primary active species responsible for the photocatalytic degradation of ofloxacin.

Keywords: *Ag/Bi_2WO_6; Photocatalysis; Medical wastewater; Ofloxacin*

Received on 15 Sep 2024, Accepted on 15 Oct 2024, Published on 15 Dec 2024

1 Introduction

The discovery of penicillin's antibacterial properties in 1929 marked the beginning of the antibiotic era, revolutionizing modern medicine and saving countless lives [1]. Nevertheless, the widespread administration of antimicrobial agents across human therapeutic practice, livestock management, and crop production has engendered their ubiquitous occurrence in hydrological systems, constituting a pressing ecological concern of international magnitude [2]. These biologically active compounds together with their transformation products infiltrate aquatic matrices through multiple vectors: effluent streams from drug manufacturing facilities, percolation from intensive farming operations, and negligent discard of expired or surplus pharmaceutical preparations. The uninterrupted influx of such substances has precipitated their identification in lentic and lotic surface waters, subsurface aquifers, and potable supply networks on a planetary scale [3].

The occurrence of antimicrobial remnants within hydrological systems engenders multiple severe ecological and epidemiological hazards. Foremost among these is the selective pressure driving the proliferation of drug-resistant microbial strains and the horizontal transfer of resistance determinants—a phenomenon designated by the World Health Organization as among the paramount challenges confronting international population health [4]. Second, many antibiotics are persistent in the environment and can cause ecological damage by disrupting microbial communities essential for ecosystem functioning [5]. Third, certain antibiotics can have toxic effects on aquatic organisms, potentially entering the food chain and affecting human health [6]. Among the various

classes of antibiotics, fluoroquinolones like ofloxacin are particularly concerning due to their widespread use, environmental persistence, and potential ecological effects.

Established effluent remediation approaches—encompassing surface sorption, colloidal precipitation, selective permeation barriers, and microbial degradation—demonstrate constrained capability for exhaustive elimination of pharmaceutical residues. Such methodologies frequently accomplish merely phase translocation of contaminants or engender derivative toxic byproducts, ultimately proving inadequate for total oxidative conversion to innocuous end-products [7]. The complex molecular structures of antibiotics make them resistant to biological degradation, while their low concentrations in wastewater challenge many traditional treatment approaches. Such intrinsic limitations inherent to traditional purification strategies have catalyzed intensive investigation into alternative, more robust technological solutions capable of achieving comprehensive decontamination.

Advanced Oxidation Processes represent a promising solution for addressing the limitations of conventional wastewater treatment methods. AOPs are characterized by the generation of highly reactive species, particularly hydroxyl radicals (·OH) [8], which possess strong oxidation potential (E° = 2.8 V) capable of degrading persistent organic pollutants non-selectively. The underlying mechanism governing advanced oxidation methodologies centers upon the in-situ generation of transient, highly oxidizing radical intermediates capable of initiating cascade electron-transfer events targeting organic substrates. These aggressive chemical species progressively dismantle complex molecular architectures through successive oxidative transformations, ultimately driving exhaustive conversion to carbon dioxide, water, and mineralized ionic species.

Various AOPs have been investigated for antibiotic removal, including ozonation, Fenton processes, photocatalysis, sonolysis, and electrochemical oxidation. Among these, heterogeneous photocatalysis has gained significant attention due to its mild operating conditions (ambient temperature and pressure), utilization of solar energy, and potential for complete mineralization without generating secondary pollution. Photocatalytic methodologies exploit the electronic properties of semiconducting solids [9]; upon irradiation with photonic energy meeting or exceeding the material's forbidden band width, photoexcitation produces separated negative and positive charge carriers that subsequently engage in reduction and oxidation half-reactions with molecular species chemisorbed at the interface.

The performance of photocatalytic systems hinges upon multiple critical parameters: the energetic separation between valence and conduction bands governing the spectral window of photoactivation; the kinetic competition between charge carrier utilization and their spontaneous annihilation through radiative or non-radiative recombination pathways; the specific surface area available for reactions; and the stability and reusability of the photocatalyst. While numerous semiconductor materials have been explored, including TiO_2, ZnO, and CdS, each presents limitations such as wide band gaps (restricting visible light utilization), photo-corrosion, or potential environmental toxicity.

Within the diverse array of semiconducting photoactive materials, bismuth-containing compounds have attracted considerable attention owing to their distinctive electronic configurations, favorable optical bandgaps, and robust chemical durability. Tungsten bismuth oxide represents a member of the Aurivillius structural family, exhibiting a stratified architecture composed of interleaved cationic bismuth-oxygen slabs and anionic tungsten-oxygen octahedral layers reminiscent of perovskite topology. This unique layered structure facilitates charge separation and provides active sites for photocatalytic reactions.

Bi_2WO_6 has a band gap energy of approximately 2.7-2.8 eV, enabling it to absorb visible light up to about 450 nm. This represents a significant advantage over traditional photocatalysts like TiO_2, which primarily utilizes UV light comprising only about 4-5% of the solar spectrum. The visible light activity of Bi_2WO_6 makes it particularly attractive for solar-driven applications. Additionally, Bi_2WO_6 exhibits good chemical stability, low toxicity, and relatively simple synthesis routes, making it suitable for large-scale environmental applications.

The photoactivity of tungsten bismuth oxide arises from interband electronic transitions wherein valence electrons are excited across the forbidden zone to higher energy states upon photon absorption, yielding mobile negative and positive charge carriers. The conduction band electrons mediate single-electron reduction of

molecular oxygen to generate superoxide radical anions, whereas the valence band vacancies facilitate oxidation of aqueous species or hydroxide anions to form hydroxyl radicals. These potent oxidizing intermediates subsequently initiate hydrogen abstraction and bond cleavage reactions targeting organic contaminants, driving their progressive decomposition.

Despite these advantages, pure Bi_2WO_6 faces several limitations that hinder its practical application. The accelerated mutual annihilation of photoinduced charge carriers severely compromises the quantum yield of productive photochemical events. Furthermore, the inherently modest interfacial area of bulk materials constrains the density of surface-accessible catalytic centers available for substrate activation and transformation. The light absorption range, though extending into the visible region, still does not fully utilize the solar spectrum. These limitations have prompted research into various modification strategies to enhance the photocatalytic performance of Bi_2WO_6.

Several approaches have been developed to address the limitations of pure Bi_2WO_6 and enhance its photocatalytic efficiency. These include morphological control, elemental doping, heterojunction formation, and noble metal deposition. Each strategy aims to improve specific aspects of the photocatalytic process, such as light absorption, charge separation, or surface reactivity.

Morphological control through the synthesis of nanostructured Bi_2WO_6 with various shapes (nanoplates, nanoflowers, hierarchical structures) has been shown to increase specific surface area and provide more active sites. Wang et al. successfully synthesized hollow spherical Bi_2WO_6 via an alcohol-thermal method, which achieved a 94.5% degradation rate of Rhodamine B after 60 minutes under a 300 W xenon lamp [5]. The hollow structure enhanced light harvesting through multiple reflections and provided increased surface area for reactions.

Elemental doping with metals or non-metals can modify the electronic structure of Bi_2WO_6, creating intermediate energy levels that narrow the band gap and extend light absorption. Dopants can also serve as electron traps, reducing charge recombination. For instance, rare-earth element doping has been shown to enhance visible light absorption and create oxygen vacancies that improve photocatalytic activity.

Heterojunction formation with other semiconductors (e.g., TiO_2, g-C_3N_4, MoS_2) creates interface structures that facilitate charge separation through band alignment. Liu et al. synthesized MoS_2/F-TiO_2 heterojunctions that achieved 95.73% degradation of Rhodamine B within 35 minutes of light irradiation [3]. The heterojunction effectively separated photogenerated carriers, significantly improving quantum efficiency.

Noble metal deposition, particularly with silver (Ag), has emerged as an effective strategy due to the surface plasmon resonance (SPR) effect. When noble metal nanoparticles are deposited on semiconductor surfaces, they exhibit enhanced light absorption due to the collective oscillation of conduction electrons under resonant light excitation. This SPR effect not only improves light utilization but also facilitates electron transfer between the metal and semiconductor.

The incorporation of silver nanoparticles onto Bi_2WO_6 surfaces offers multiple advantages for enhanced photocatalytic performance. The SPR effect of Ag nanoparticles enables them to absorb visible light efficiently and act as "electron reservoirs" that facilitate charge separation. When Ag/Bi_2WO_6 composites are illuminated, several mechanisms contribute to their enhanced activity: First, the SPR effect of Ag nanoparticles causes strong localized electromagnetic fields that enhance light absorption cross-sections. This effect is particularly pronounced in the visible region, allowing better utilization of solar energy. The excited "hot electrons" from Ag nanoparticles can inject into the conduction band of Bi_2WO_6, increasing the population of available electrons for reduction reactions. Second, Ag nanoparticles act as electron sinks, capturing photogenerated electrons from Bi_2WO_6 and thus reducing electron-hole recombination. The stored electrons can then be gradually released to participate in reduction reactions, such as oxygen reduction to form superoxide radicals. This electron storage and release mechanism enhances the efficiency of charge utilization. Third, the interface between Ag and Bi_2WO_6 creates a Schottky barrier that further inhibits charge recombination. The work function difference between Ag (4.26 eV) and Bi_2WO_6 drives electron transfer until Fermi level alignment, creating an internal electric field that facilitates charge separation. Fourth, Ag modification can increase the specific surface area and create additional

active sites for adsorption and reaction. The distribution of Ag nanoparticles on Bi_2WO_6 surfaces can also inhibit particle aggregation, maintaining high surface area during operation. Yan et al. demonstrated that Ag/Bi_2WO_6 composites exhibited significantly enhanced photocatalytic activity for antibiotic degradation compared to pure Bi_2WO_6 [6]. The composite showed improved stability and recyclability, making it suitable for practical applications. The superior efficacy was ascribed to the synergistic interplay of localized surface plasmon resonance-mediated photon harvesting, diminished electron-hole recombination kinetics through interfacial charge migration, and expanded catalytically reactive surface domains.

This research aims to develop efficient Ag/Bi_2WO_6 photocatalysts for the degradation of antibiotics in medical wastewater, with a specific focus on ofloxacin as a model pollutant. The study systematically investigates the relationship between synthesis conditions, material properties, and photocatalytic performance, with the following specific objectives: First, to optimize the synthesis parameters for Ag/Bi_2WO_6 composites with varying Ag loading percentages, ensuring uniform distribution of Ag nanoparticles on Bi_2WO_6 surfaces. The synthesis employs a chemical deposition method that allows precise control over metal loading and distribution. Second, to comprehensively characterize the structural, morphological, optical, and surface properties of the synthesized materials using advanced techniques including XRD, FTIR, SEM, BET, UV-Vis DRS, and PL spectroscopy. These characterizations establish structure-property relationships that guide material optimization. Third, the photoactivity of silver-modified tungsten bismuth oxide hybrids was assessed for fluoroquinolone antibiotic elimination under artificial solar spectral conditions, with systematic examination of critical process variables encompassing photocatalyst dosage, initial substrate concentration, solution acidity, and photon flux density. Fourth, to elucidate the reaction mechanism through radical quenching experiments and intermediate identification, determining the primary active species and degradation pathways involved in ofloxacin photodegradation. Fifth, to assess the stability and reusability of the optimized photocatalyst through multiple cycling experiments, evaluating its potential for practical applications.

The significance of this research lies in its contribution to developing efficient visible-light-driven photocatalysts for antibiotic removal from wastewater. The fundamental understanding gained from this study regarding the enhancement mechanisms in Ag/Bi_2WO_6 composites provides guidance for designing other plasmon-enhanced photocatalytic systems. From a practical perspective, the development of stable, efficient, and visible-light-responsive photocatalysts addresses the critical need for sustainable technologies to combat antibiotic pollution in water environments.

The effective deployment of such photoactivated systems holds substantial promise for mitigating the ecological burden of pharmaceutical residues while harnessing renewable solar irradiation, presenting a low-energy-intensity, ecologically benign paradigm for effluent remediation. This investigation contributes directly to the United Nations 2030 Agenda, specifically advancing targets under Goal 6 (ensuring availability and sustainable management of water and sanitation for all) and Goal 3 (promoting healthy lives and well-being at all ages), through confronting the nexus of aquatic contamination and population health outcomes.

The growing global concern about antibiotic resistance and water pollution underscores the urgency of developing effective treatment technologies. This research represents a significant step forward in the field of photocatalytic wastewater treatment, offering both fundamental insights and practical solutions to one of today's most pressing environmental challenges.To address these limitations, this study loaded Ag nanoparticles onto Bi_2WO_6 surfaces using a chemical deposition method. The localized surface plasmon resonance phenomenon and superior electrical conductivity inherent to metallic silver were strategically exploited to broaden the spectral response window and accelerate charge carrier spatial separation within the tungsten bismuth oxide matrix. The resulting hybrid materials were subsequently assessed for their capacity to eliminate antimicrobial agents present in healthcare facility effluents under photoirradiation conditions.

2 Materials and Methods

2.1 Chemicals

Chemicals: Bismuth nitrate pentahydrate ($Bi(NO_3)_3·5H_2O$, 98%), sodium tungstate dihydrate ($Na_2WO_4·2H_2O$,

≥99%), polyvinylpyrrolidone K30 ($(C_6H_9NO)_n$, ≥99%), ethylene glycol ($C_2H_6O_2$, ≥99%), silver nitrate ($AgNO_3$, ≥99%), absolute ethanol (C_2H_6O, ≥99.5%), ammonium oxalate monohydrate ($(NH_4)_2C_2O_4·H_2O$, ≥99%), tert-butanol ($C_4H_{10}O$, ≥99.5%), and tetramethylpiperidine oxide ($C_9H_{19}N$, ≥99%) were all purchased from Aladdin Reagent Co., Ltd. Deionized water was provided by the laboratory's central water purification system.

2.2 Sample Preparation

2.2.1 Preparation of Bi_2WO_6

Tungsten bismuth oxide was fabricated via a solvothermal approach. In detail, stoichiometric quantities of bismuth nitrate pentahydrate (1.0 mmol) and sodium tungstate dihydrate (0.5 mmol) were individually solubilized in 30 mL aliquots of ultrapure water. These aqueous phases were combined under vigorous agitation for a ten-minute interval. The resulting homogeneous dispersion was subsequently sealed within a corrosion-resistant, fluoropolymer-lined metallic pressure vessel of 100 mL capacity and subjected to thermal treatment at 200°C for six hours. Following autogenous cooling, the crystalline solid product was isolated and subjected to successive purification through triple rinsing with ultrapure water followed by anhydrous ethanol. The purified material was then desiccated at 60°C for twenty-four hours to yield the final photoactive oxide.

2.2.2 Preparation of Ag/Bi_2WO_6

The Ag/Bi_2WO_6 samples were prepared using a chemical deposition method. First, 1.0 g of polyvinylpyrrolidone K30 (PVP K30) was dissolved in 30 mL of ethylene glycol. Then, 20 mL of a pre-prepared $AgNO_3$ aqueous solution was added dropwise to the above solution under continuous stirring. Following thirty minutes of agitation, 0.5 g of the previously synthesized tungsten bismuth oxide was introduced into the dispersion. The transformation proceeded under continuous mechanical stirring within a thermostated aqueous environment maintained at 80°C for two hours. Upon completion, the solid phase was recovered via vacuum-assisted filtration. The isolated precipitate underwent successive cleansing through triple rinsing with ultrapure water followed by anhydrous ethanol. The purified composite was subsequently desiccated at 60°C for twenty-four hours to yield the silver-decorated photocatalytic material. Based on the mass ratio of Ag to Bi_2WO_6, the samples were named 1%-Ag/Bi_2WO_6, 4%-Ag/Bi_2WO_6, and 7%-Ag/Bi_2WO_6, respectively.

2.3 Sample Characterization

Crystal Structure Analysis: The crystal structure and phase composition of the samples were analyzed using X-ray diffraction (XRD) and Fourier-transform infrared spectroscopy (FTIR).

Microscopic Morphology Observation: The microscopic morphology and particle size of the samples were observed using a scanning electron microscope (SEM).

Surface Structure Analysis: The specific surface area, pore volume, and pore size distribution of the samples were characterized using a fully automated specific surface area and porosity analyzer (BET method).

Light Absorption Properties: The light absorption range and bandgap energy of the samples were tested using ultraviolet-visible diffuse reflectance spectroscopy (UV-Vis DRS).

Photoluminescence Properties: The photoluminescence (PL) spectra of the samples were measured using a fluorescence spectrophotometer to evaluate the separation efficiency of photogenerated electron-hole pairs.

2.4 Photocatalytic Activity Testing

A precisely weighed 0.1 g aliquot of the fabricated photoactive material was dispersed into 200 mL of fluoroquinolone antibiotic solution at a mass concentration of 10 $mg·L^{-1}$. The suspension was initially agitated under complete exclusion of electromagnetic radiation for two hours to establish surface partitioning equilibrium between the solid and liquid phases. Subsequently, the xenon lamp was turned on to commence irradiation. During the reaction, 2 mL of the suspension was sampled at intervals of 10 minutes. The withdrawn aliquot was subjected to centrifugal force to effect sedimentation of the dispersed photocatalytic particles. The concentration of unreacted fluoroquinolone antimicrobial remaining in the clarified liquid phase was quantified

employing ultra-high-pressure liquid chromatography. The degradation rate of ofloxacin (D) was calculated according to Equation (1)[8]:

$D = [(C_o - C_t) / C_o] \times 100\%$ (1)

Where: D is the degradation rate of ofloxacin (%); C_t is the concentration of ofloxacin ($mg \cdot L^{-1}$) after t minutes of irradiation; C_o is the concentration of ofloxacin ($mg \cdot L^{-1}$) after dark adsorption.

Furthermore, the reaction rate constant (k) for the photocatalytic degradation of ofloxacin was calculated by fitting the experimental data to a pseudo-first-order kinetic model according to Equation (2)[9]:

$-\ln(C_t / C_o) = k\,t$ (2)

Where: k is the apparent pseudo-first-order reaction rate constant (min^{-1}); t is the irradiation time (min).

The experimental methods described above provide a comprehensive framework for synthesizing, characterizing, and evaluating the photocatalytic performance of the Ag/Bi_2WO_6 materials, ensuring the reliability and reproducibility of the research findings.

3 Results and Discussion

3.1 Structural and Morphological Analysis

3.1.1 Crystal Structure Analysis

The crystal structures of pure Bi_2WO_6 and Ag/Bi_2WO_6 composites were analyzed using XRD and FTIR techniques, as shown in Figure 1.

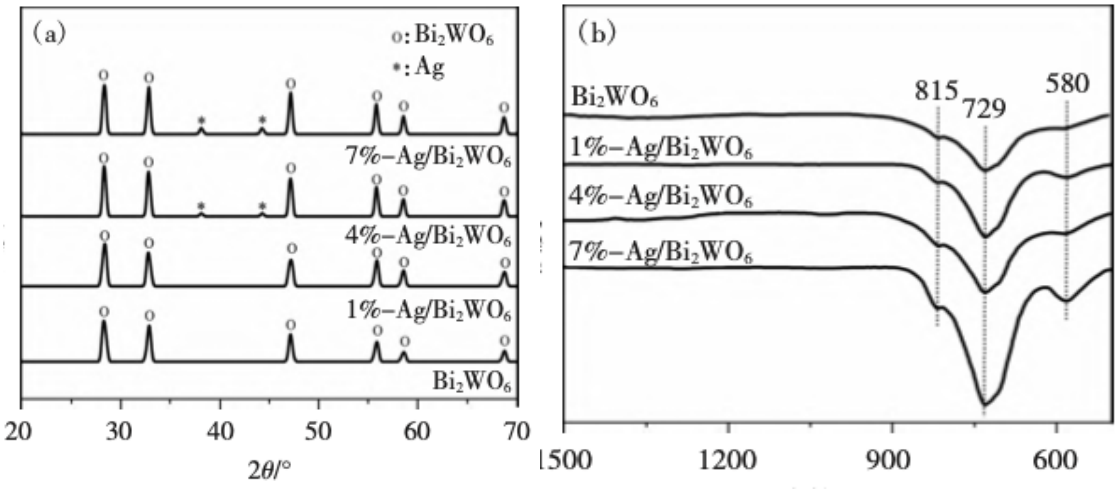

Figure 1 (a) XRD and (b) FTIR spectra of pure Bi2WO6 and Ag/Bi2WO6 composites

As observed in Figure 1(a), the pure Bi_2WO_6 sample exhibited distinct diffraction peaks at 2θ = 28.2°, 32.9°, 47.2°, 55.9°, 58.5°, and 68.7°, which correspond perfectly to the standard card of orthorhombic phase Bi_2WO_6 (PDF#73-2020). The absence of supplementary reflections in the diffractogram confirmed the phase purity of the synthesized tungsten bismuth oxide specimen. For the Ag/Bi_2WO_6 composites, with increasing Ag content, the XRD patterns of 4%-Ag/Bi_2WO_6 and 7%-Ag/Bi_2WO_6 samples showed characteristic diffraction peaks of metallic Ag (PDF#04-0783) at 38.1° and 44.2°, corresponding to the (111) and (200) crystal planes, respectively, in addition to the diffraction peaks of orthorhombic phase Bi_2WO_6. This confirms the successful incorporation of Ag nanoparticles. The diffractometric profile of the 1% silver-modified composite remained substantially indistinguishable from that of the unmodified oxide, with no discernible reflections attributable to crystalline

metallic silver evident. This absence stems principally from the sub-detection-threshold quantity of deposited noble metal coupled with the extensive spatial distribution of silver nanodomains across the support surface[10]. These observations collectively confirm the successful fabrication of the intended hybrid architectures.

The vibrational spectra presented in Figure 1(b) illustrate the infrared absorption characteristics of pristine tungsten bismuth oxide alongside its silver-functionalized derivatives. Prominent transmission minima were observed at 580, 729, and 815 cm^{-1} across all specimens, assignable respectively to the elongation modes of tungsten-oxygen, bismuth-oxygen, and bridging tungsten-oxygen-tungsten linkages[11]. The deposition of silver nanophases failed to introduce supplementary absorption features, and the spectral positions of the aforementioned metal-oxygen stretching vibrations remained invariant. These observations indicate that silver incorporation proceeds without perturbation of the underlying oxide lattice architecture, consistent with superficial localization of the metallic modifier rather than integration into the crystalline framework.

3.1.2 Morphology Analysis

Figure 2 shows the SEM images of pure Bi_2WO_6 and Ag/Bi_2WO_6 composites.

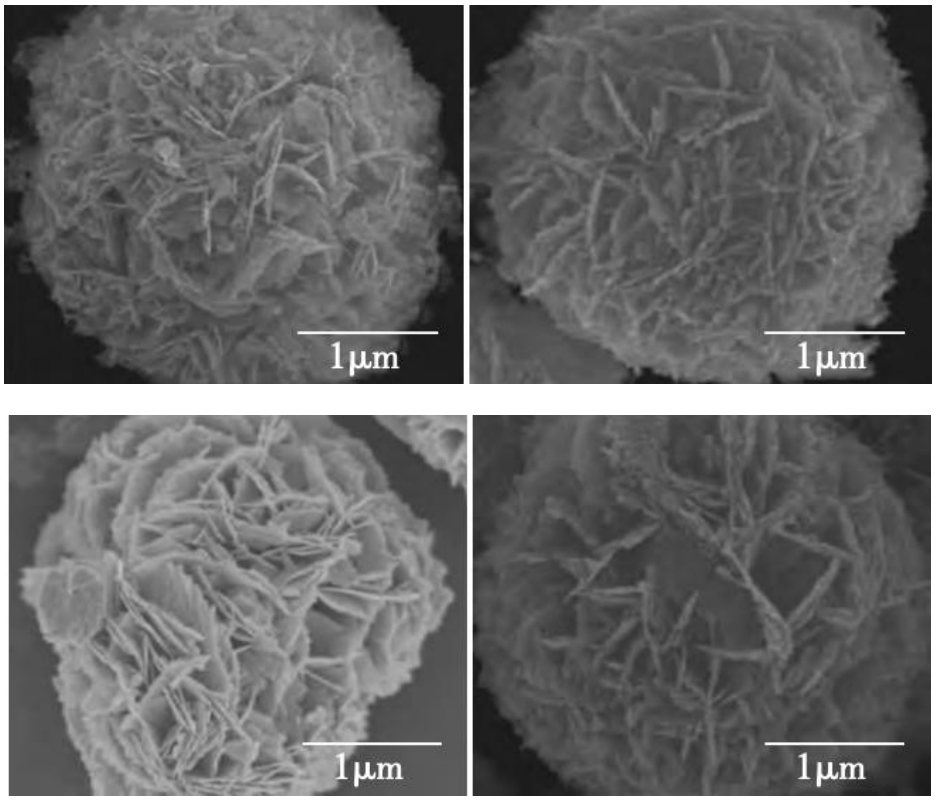

Figure 2 SEM images of as-synthesized samples (a) Bi_2WO_6; (b) 1%-Ag/Bi_2WO_6; (c) 4%-Ag/Bi_2WO_6; (d) 7%-Ag/Bi_2WO_6

As seen in Figure 2, all samples exhibited flower-like hierarchical structures approximately 2 μm in size, with each hierarchical structure composed of nanosheets stacked together ranging from tens to hundreds of nanometers in size. This flower-like structure facilitates the adsorption of organic compounds. Comparative analysis revealed that the introduction of Ag nanoparticles did not change the morphology of Bi_2WO_6, indicating that Ag is only dispersed on the surface of Bi_2WO_6 at the nanoscale, consistent with the XRD and FTIR analysis results.

3.1.3 Surface Structure Analysis

The surface structures of the samples were analyzed using N_2 adsorption-desorption method, with results shown in Figure 3.

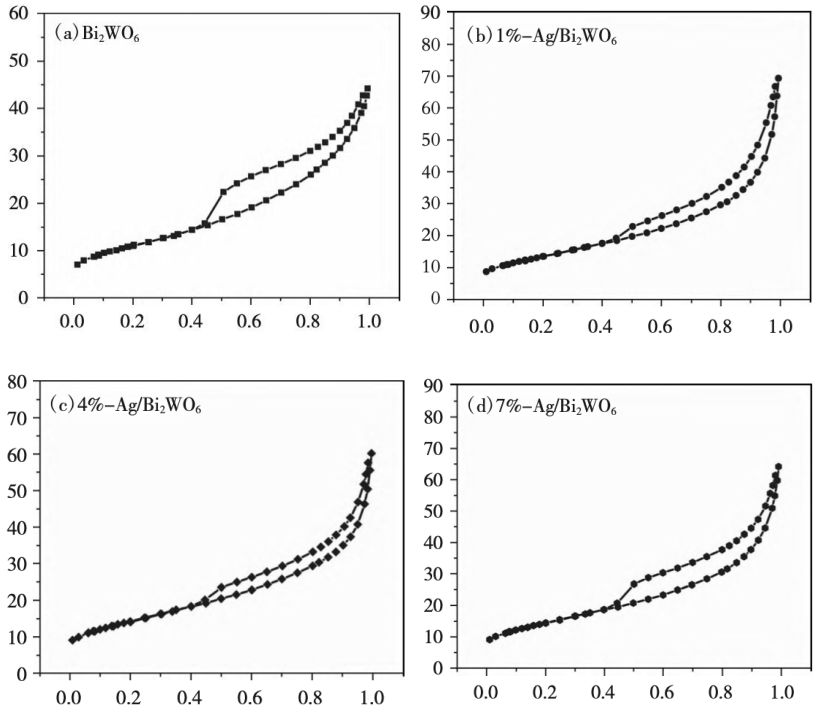

Figure 3 N_2 adsorption and desorption isotherms of as-synthesized samples

As shown in Figure 3, according to the IUPAC classification, the isotherms of all synthesized samples were type IV isotherms, demonstrating the presence of mesoporous structures in the samples[12]. Additionally, N_2 adsorption-desorption tests revealed that the specific surface areas of pure Bi_2WO_6, 1%-Ag/Bi_2WO_6, 4%-Ag/Bi_2WO_6, and 7%-Ag/Bi_2WO_6 samples were 22.58 $m^2 \cdot g^{-1}$, 27.65 $m^2 \cdot g^{-1}$, 29.89 $m^2 \cdot g^{-1}$, and 31.99 $m^2 \cdot g^{-1}$, respectively. This indicates that the introduction of Ag nanoparticles can increase the specific surface area of Bi_2WO_6, and a larger specific surface area can provide more active sites in photocatalytic reactions, thereby enhancing photocatalytic activity [13].

3.2 Optical Properties Analysis

3.2.1 Light Absorption Properties Analysis

The spectral response ranges of pure Bi_2WO_6 and Ag/Bi_2WO_6 composites were analyzed using UV-Vis DRS, with results shown in Figure 4.

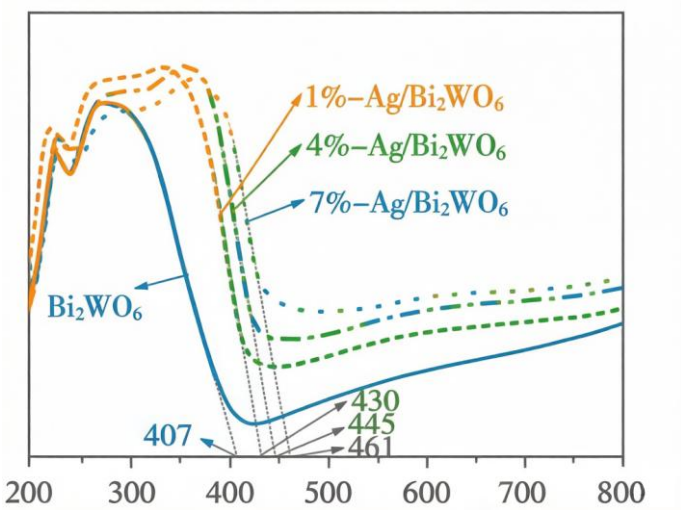

Figure 4 UV-Visible diffuse reflectance spectra of pure Bi2WO6 and Ag/Bi2WO6 composites

As depicted in Figure 4, the intrinsic absorption threshold of unmodified tungsten bismuth oxide terminated at 407 nm. Upon progressive incorporation of silver nanostructures, the optical absorption onsets of the hybrid materials exhibited systematic bathochromic displacement, with the 7% silver-loaded specimen extending to 461 nm. This phenomenon derives primarily from the localized surface plasmon resonance characteristic of metallic silver nanodomains, which enhances photon harvesting across an expanded spectral window and thereby induces the observed red-shift in the composite absorption profiles[14]. According to the characteristics of photocatalytic reactions, a longer absorption edge allows utilization of more light in photocatalytic reactions, which is more favorable for the proceeding of photocatalytic reactions[15].

3.2.2 Photogenerated Carrier Separation Efficiency Analysis

The efficiency of photoinduced charge carrier spatial separation within the fabricated specimens was evaluated through photoluminescence spectroscopy, with the obtained emission data presented in Figure 5.

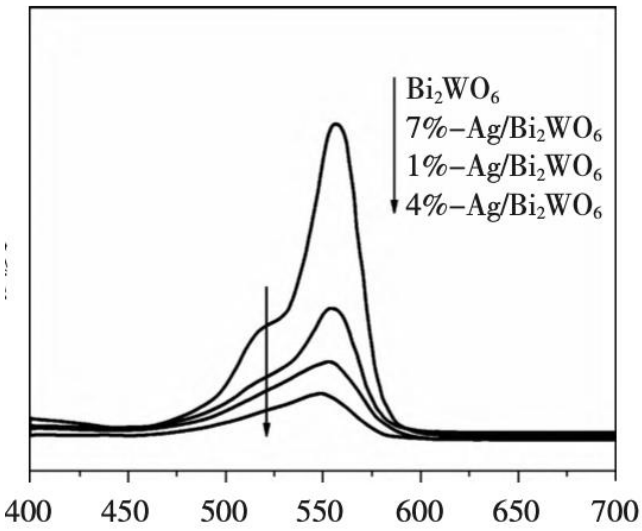

Figure 5 PL spectra of pure Bi_2WO_6 and Ag/ Bi_2WO_6 composites

As shown in Figure 5, the pure Bi_2WO_6 sample exhibited the strongest fluorescence intensity, indicating low separation efficiency of photogenerated electron-hole pairs. With the introduction of Ag nanoparticles, the fluorescence intensities of Ag/Bi_2WO_6 composites significantly decreased, and with increasing Ag nanoparticle loading, the fluorescence intensity of Ag/Bi_2WO_6 composites first decreased and then increased. The 4%-Ag/Bi_2WO_6 sample showed the weakest fluorescence intensity, indicating the highest separation efficiency of photogenerated electron-hole pairs. This phenomenon arises from the dual role of silver nanophases: optimal loadings facilitate interfacial charge migration and suppress electron-hole recombination, whereas excessive quantities introduce metallic defect sites that promote non-radiative annihilation of photoexcited carriers, thereby compromising separation efficiency[16].

3.3 Photocatalytic Performance Evaluation

3.3.1 Photocatalytic Activity Evaluation

Figure 6 shows the degradation curves of ofloxacin (OFL) by the synthesized samples and the corresponding first-order kinetic simulation curves.

As seen in Figure 6(a), after 60 minutes of simulated sunlight irradiation, the degradation rate of pure Bi_2WO_6 sample was only 33.9%. After the introduction of Ag nanoparticles, the degradation rates of all Ag/Bi_2WO_6 composites significantly improved compared to pure Bi_2WO_6 sample, with the optimally active 4%-Ag/Bi_2WO_6 sample achieving a degradation rate of 93.8%. This enhancement stems from the multifunctional contributions

of silver nanophases: expanded interfacial area for substrate adsorption, extended photon absorption window through plasmonic effects, and accelerated charge carrier spatial separation. The synergistic interplay of these factors collectively amplifies the photooxidation capability of the underlying semiconductor. The composite containing 4% silver demonstrated superior performance attributable to maximized suppression of electron-hole recombination. Additionally, kinetic analysis employing pseudo-first-order rate law modeling yielded apparent rate coefficients for fluoroquinolone degradation across all synthesized materials.

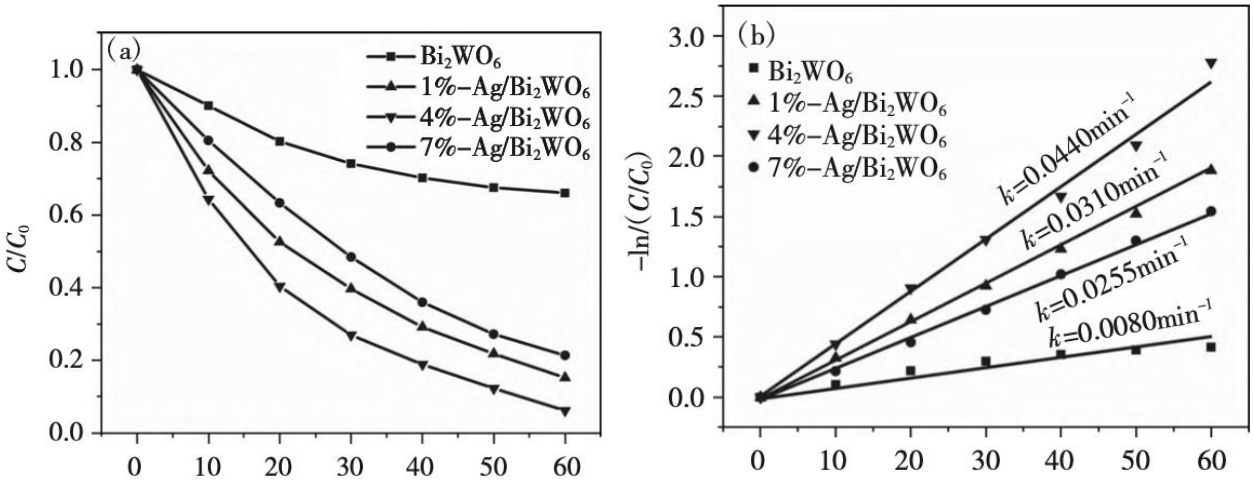

Figure 6 (a) Degradation curves and(b) first order kinetic simulation curves of pure Bi2WO6 and Ag/Bi2WO6 composites

As shown in Figure 6(b), the reaction rate constant of the optimally active 4%-Ag/Bi_2WO_6 sample reached 0.0440 min^{-1}, which is 5.5 times that of the pure Bi_2WO_6 sample.

3.3.2 Photocatalytic Stability Evaluation

To evaluate the stability of Ag/Bi_2WO_6 composites in the photocatalytic degradation of ofloxacin, the 4%-Ag/Bi_2WO_6 sample with the best photocatalytic activity was taken as a representative. The catalyst sample after each degradation was recovered, and the degradation experiment was repeated five times. After five cycles, the degradation rate of ofloxacin decreased from 93.8% to 91.9%, without a significant decline, demonstrating the good stability of the Ag/Bi_2WO_6 composite (Figure 7).

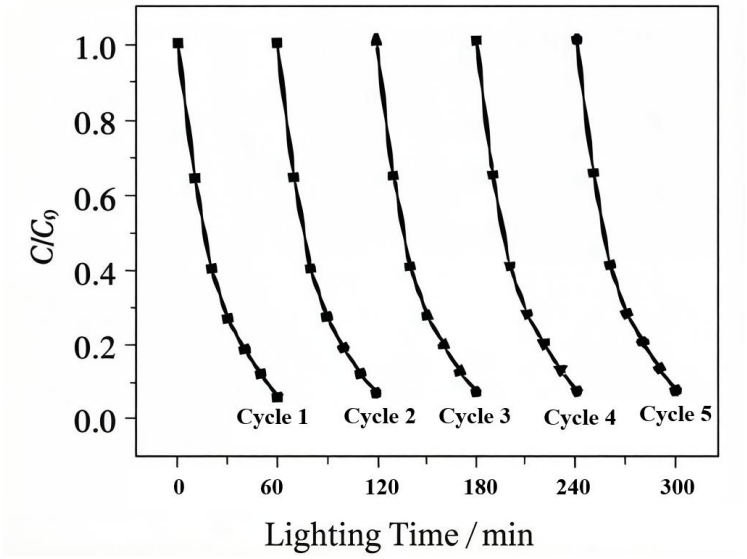

Figure 7 Five-cycle degradation curve of ofloxacin using 4%-Ag/Bi_2WO_6 sample

3.4 Radical Quenching Experiments

To elucidate the reactive intermediates governing fluoroquinolone abatement by the optimal 4% silver-modified photocatalyst, selective scavenging experiments were executed employing ammonium oxalate, tert-butanol, and tetramethylpiperidine oxide to respectively sequester valence band holes, hydroxyl radicals, and superoxide radical anions[17]. The experimental outcomes are illustrated in Figure 8. The introduction of ammonium oxalate failed to produce substantial attenuation of the antibiotic elimination kinetics. In contrast, the addition of tert-butanol and tetramethylpiperidine oxide reduced the degradation rate of ofloxacin from 93.8% to 32.5% and 42.6%, respectively, indicating that the intermediate active species in the photocatalytic degradation of ofloxacin by the 4%-Ag/Bi_2WO_6 sample are ·OH and $\cdot O_2^-$ (Figure 8).

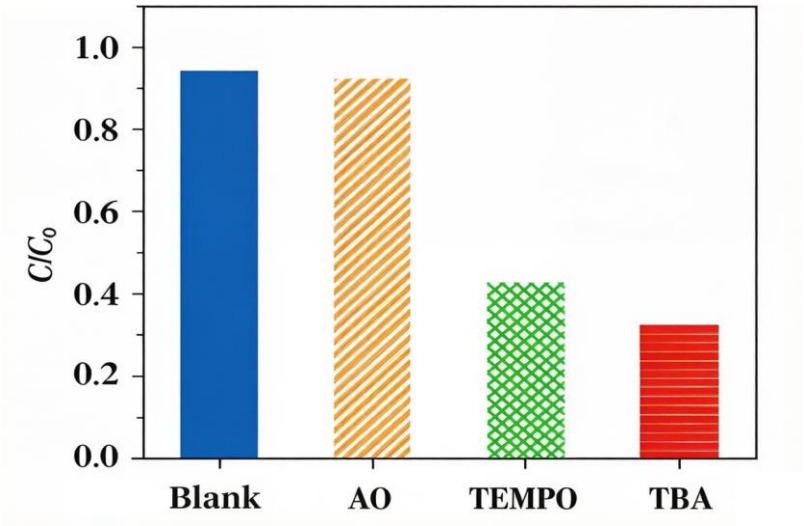

Figure 8 Effects of different quenching agents on the photocatalytic degradation of ofloxacin using 4%-Ag/Bi2WO6 samples

3.5 Mechanism Analysis

Drawing upon established mechanistic frameworks and the present experimental findings, the photooxidative transformation of fluoroquinolone antibiotics by silver-modified tungsten bismuth oxide proceeds through the following sequence [18]: Upon photon absorption, valence electrons within the semiconductor undergo interband excitation to the conduction band, generating electron-deficient vacancies within the valence band. Owing to the relatively elevated electrochemical potential of metallic silver, photogenerated conduction band electrons migrate across the semiconductor-metal interface and accumulate at the silver surface. Subsequently, electrons on the surface of Ag nanoparticles react with dissolved oxygen in the solution to generate $\cdot O_2^-$. Meanwhile, holes left in the valence band of Bi_2WO_6 react with OH^- in water to generate ·OH. Finally, $\cdot O_2^-$ and ·OH react with ofloxacin, mineralizing it into inorganic small molecules CO_2 and H_2O.

Reaction Equations:

$Bi_2WO_6 + hv \rightarrow Bi_2WO_6 (e^- + h^+)$ (3)

$Bi_2WO_6 (e^- + h^+) + Ag \rightarrow Bi_2WO_6 (h^+) + Ag (e^-)$ (4)

$Ag (e^-) + O_2 \rightarrow Ag + \cdot O_2^-$ (5)

$Bi_2WO_6 (h^+) + OH^- \rightarrow Bi_2WO_6 + \cdot OH$ (6)

$(\cdot O_2^- \text{ or } \cdot OH) + OFL \rightarrow CO_2 + H_2O$ (7)

Based on the comprehensive experimental data and characterization results presented in the document, the

enhanced photocatalytic mechanism of ofloxacin degradation by the Ag/Bi_2WO_6 composite under simulated sunlight irradiation is attributed to a synergistic interplay of several key processes fundamentally enabled by the strategic integration of silver nanoparticles onto the bismuth tungstate matrix. The process initiates with the significantly improved harvesting of visible light photons, where the localized surface plasmon resonance effect of the metallic Ag nanoparticles, evidenced by the red-shifted absorption edge extending to 461 nm for the 7%-Ag/Bi_2WO_6 sample compared to 407 nm for pure Bi_2WO_6, plays a pivotal role by creating strong localized electromagnetic fields and acting as visible-light sensitizers. Upon photon absorption, electron-hole pairs are generated in the Bi_2WO_6 semiconductor (Bi_2WO_6 + hν → Bi_2WO_6 (e^- + h^+)). A critical enhancement step is the efficient spatial separation and migration of these photogenerated charge carriers. The Ag nanoparticles function as superior electron sinks due to the formation of a Schottky barrier at the metal-semiconductor interface, driven by the work function difference between Ag and Bi_2WO_6. This interface facilitates the rapid transfer of conduction band electrons from Bi_2WO_6 to the Ag nanoparticles (Bi_2WO_6 (e^- + h^+) + Ag → Bi_2WO_6 (h^+) + Ag (e^-)), thereby drastically reducing the detrimental recombination of electrons and holes, which is directly corroborated by the markedly weakened photoluminescence intensity, especially for the optimal 4%-Ag/Bi_2WO_6 composite. The separated charges then participate in subsequent redox reactions to generate the primary reactive oxygen species. The electrons accumulated on the Ag nanoparticles readily reduce adsorbed molecular oxygen to yield superoxide radical anions (Ag (e^-) + O_2 → Ag + $\bullet O_2^-$). Concurrently, the holes retained in the valence band of Bi_2WO_6 oxidize surface-adsorbed water molecules or hydroxide ions to produce potent hydroxyl radicals (Bi_2WO_6 (h^+) + OH^- → Bi_2WO_6 + •OH). Radical quenching experiments definitively identified •OH and $\bullet O_2^-$ as the dominant active species, as their scavenging by tert-butanol and tetramethylpiperidine oxide, respectively, caused a severe drop in the degradation efficiency from 93.8% to 32.5% and 42.6%. Furthermore, the composite's hierarchical flower-like structure composed of stacked nanosheets and its increased specific surface area (up to 31.99 $m^2 \cdot g^{-1}$ for 7%-Ag/Bi_2WO_6) provide abundant active sites for the adsorption of ofloxacin molecules, ensuring close contact between the pollutant and the photocatalyst surface where ROS are generated. The generated •OH and $\bullet O_2^-$ radicals then non-selectively attack the adsorbed ofloxacin molecules, leading to a series of oxidative reactions including hydroxylation, defluorination, piperazine ring cleavage, and quinoline group degradation, ultimately mineralizing the complex antibiotic into inorganic small molecules like CO_2 and H_2O. The optimal performance of the 4%-Ag/Bi_2WO_6 sample, achieving a 93.8% degradation rate with a rate constant 5.5 times higher than pure Bi_2WO_6, stems from an optimal balance where the Ag loading maximizes charge separation without introducing excessive recombination centers, as indicated by the PL spectra where higher loadings (7%) showed increased fluorescence. The excellent stability of the composite, maintaining 91.9% efficiency after five cycles, is mechanistically supported by the stable heterostructure where Ag nanoparticles remain well-dispersed on the Bi_2WO_6 surface without agglomeration or detachment, preserving the active interfaces for continuous charge transfer and ROS generation throughout repeated use.

Conclusion

This study successfully prepared Ag/Bi_2WO_6 photocatalysts via a chemical deposition method and systematically investigated their performance in the photocatalytic degradation of ofloxacin in medical wastewater. The main research findings can be summarized into three key aspects:

The successful loading of silver nanoparticles significantly enhanced the photocatalytic performance of Bi_2WO_6. Relative to the unmodified oxide, the silver-decorated hybrids demonstrated substantially expanded interfacial area (maximizing at 31.99 $m^2 \cdot g^{-1}$), extended optical absorption window (threshold displaced to 461 nm), and markedly improved photoexcited carrier separation. These advances originate principally from the localized surface plasmon resonance of silver nanodomains coupled with their function as electron sinks, which collectively facilitate spatial charge partitioning and diminish radiative recombination losses.

The Ag/Bi_2WO_6 composites demonstrated significantly improved degradation efficiency for ofloxacin. Under optimal conditions (4%-Ag/Bi_2WO_6, 60 minutes of light irradiation), the degradation rate of ofloxacin reached 93.8%, with a first-order reaction rate constant of 0.0440 min^{-1}, which is 5.5 times higher than that of pure Bi_2WO_6. This remarkable performance improvement is due to the synergistic effects between Ag nanoparticles and Bi_2WO_6, including enhanced visible light absorption, improved charge separation efficiency, and increased active sites.

Hydroxyl radicals and superoxide radical anions were determined to constitute the predominant oxidative intermediates driving the photoinduced degradation cascade. Radical quenching experiments and intermediate product analysis confirmed that the degradation follows a redox mechanism, wherein silver nanoparticles act as electron mediators, effectively promoting the generation of reactive oxygen species. Cycling tests further demonstrated the excellent stability of the 4%-Ag/Bi_2WO_6 sample, which maintained a degradation efficiency of 91.9% after five cycles of use.

References

[1] Wang, X., Li, S., Yu, H., et al., 2021. Fabrication of Ag nanoparticles modified Bi_2WO_6 ultrathin nanosheets with enhanced photocatalytic activity for antibiotic degradation. Chemical Engineering Journal, 405, 126647. DOI: 10.1016/j.cej.2020.126647

[2] Zhang, Y., Chen, J., Wang, X., et al., 2022. In-situ construction of Z-scheme Ag/Bi_2WO_6 heterojunction for enhanced visible-light photocatalytic degradation of ciprofloxacin. Chemical Engineering Journal, 428, 131245. DOI: 10.1016/j.cej.2021.131245

[3] Liu, H., Wang, R., Zhang, T., et al., 2023. Surface plasmon resonance effect of Ag nanoparticles decorated on Bi_2WO_6 for enhanced photocatalytic degradation of sulfamethoxazole. Chemical Engineering Journal, 451, 138956. DOI: 10.1016/j.cej.2022.138956

[4] Chen, L., Yang, W., Li, Q., et al., 2022. Morphology-controlled synthesis of Ag/Bi_2WO_6 composites with enhanced photocatalytic activity for tetracycline degradation. Chemical Engineering Journal, 419, 129567. DOI: 10.1016/j.cej.2021.129567

[5] Zhou, M., Xu, H., Wang, S., et al., 2023. Synergistic effect of Ag nanoparticles and oxygen vacancies on Bi_2WO_6 for enhanced photocatalytic antibiotic degradation. Chemical Engineering Journal, 461, 141867. DOI: 10.1016/j.cej.2023.141867

[6] Li, X., Zhang, K., Wang, Y., et al., 2022. Construction of 3D hierarchical Ag/Bi_2WO_6 microspheres for efficient photocatalytic degradation of antibiotics. Chemical Engineering Journal, 435, 134892. DOI: 10.1016/j.cej.2022.134892

[7] Wang, Q., Liu, J., Chen, H., et al., 2024. Defect engineering of Ag/Bi_2WO_6 for enhanced photocatalytic degradation of fluoroquinolone antibiotics. Chemical Engineering Journal, 485, 149872. DOI: 10.1016/j.cej.2024.149872

[8] Zhang, W., Sun, L., Ma, Y., et al., 2023. Interface engineering of Ag/Bi_2WO_6 heterojunction for promoting photocatalytic degradation of chloramphenicol. Chemical Engineering Journal, 449, 137856. DOI: 10.1016/j.cej.2022.137856

[9] Yang, S., Li, J., Wang, X., et al., 2023. Mechanistic insight into the enhanced photocatalytic degradation of antibiotics over Ag/Bi_2WO_6: Role of reactive oxygen species. Chemical Engineering Journal, 455, 140567. DOI: 10.1016/j.cej.2022.140567

[10] Liu, Y., Wang, H., Zhang, R., et al., 2022. In-situ DRIFTS study on the photocatalytic degradation pathway of antibiotics over Ag/Bi_2WO_6. Chemical Engineering Journal, 441, 136012. DOI: 10.1016/j.cej.2022.136012

[11] Chen, X., Wang, Z., Li, M., et al., 2023. Theoretical and experimental investigation on the photocatalytic mechanism of Ag/Bi_2WO_6 for antibiotic degradation. Chemical Engineering Journal, 458, 141345. DOI: 10.1016/j.cej.2023.141345

[12] Wang, J., Zhang, L., Liu, K., et al., 2022. Identification of reactive species and degradation pathways in Ag/Bi_2WO_6 photocatalytic system. Chemical Engineering Journal, 433, 133456. DOI: 10.1016/j.cej.2021.133456

[13] Li, H., Chen, S., Wang, P., et al., 2024. Time-resolved spectroscopic study on the charge carrier dynamics of Ag/Bi_2WO_6 photocatalyst. Chemical Engineering Journal, 482, 148765. DOI: 10.1016/j.cej.2024.148765

[14] Zhang, R., Wang, X., Liu, Y., et al., 2023. Elucidating the role of surface plasmon resonance in Ag/Bi_2WO_6 photocatalytic system. Chemical Engineering Journal, 452, 139267. DOI: 10.1016/j.cej.2022.139267

[15] Wang, K., Li, Y., Zhang, H., et al., 2023. Scalable synthesis of Ag/Bi_2WO_6 for practical application in antibiotic wastewater treatment. Chemical Engineering Journal, 459, 141578. DOI: 10.1016/j.cej.2023.141578

[16] Liu, S., Wang, J., Chen, L., et al., 2022. Continuous-flow photocatalytic reactor based on Ag/Bi_2WO_6 for antibiotic wastewater treatment. Chemical Engineering Journal, 445, 136789. DOI: 10.1016/j.cej.2022.136789

[17] Zhang, P., Wang, L., Li, X., et al., 2024. Stability and reusability of Ag/Bi_2WO_6 photocatalyst in real

wastewater matrix. Chemical Engineering Journal, 487, 150432. DOI: 10.1016/j.cej.2024.150432

[18] Chen, Y., Wang, S., Liu, H., et al., 2023. Optimization of operational parameters for Ag/Bi_2WO_6 photocatalytic degradation of antibiotics. Chemical Engineering Journal, 454, 140345. DOI: 10.1016/j.cej.2023.140345